

# Vortex lattice in presence of a tunable periodic pinning potential

W. V. Pogosov<sup>a</sup>, A. L. Rakhmanov<sup>b</sup>, and V. V. Moshchalkov<sup>c</sup>

<sup>a</sup> *Moscow Institute of Physics and Technology, 141700  
Dolgoprudny, Moscow region, Russia*

<sup>b</sup> *Institute for Theoretical and Applied Electrodynamics,  
Russian Academy of Sciences, 127412, Moscow, Russia*

<sup>c</sup> *Laboratorium voor Vaste-Stoffysica en Magnetisme, K.U. Leuven,  
Celestijnenlaan 200 D, B-3001 Leuven, Belgium*

(March 22, 2022)

The vortex patterns stabilized by the square array of artificial pinning sites with a tunable pinning strength are studied by using a phenomenological approach in the London limit. The transitions between pinned and deformed triangular lattices are analyzed as a function of the amplitude of the vortex-pinning site interaction and the characteristic length-scale of this interaction. The critical current and different phases of vortex lattice are studied in presence of external transport current.

PACS numbers: 74.20.De, 74.60.Ec, 74.25.Ha

## I. INTRODUCTION

Nanoengineered periodic pinning arrays (PPA) have attracted recently a lot of attention [1–9]. By using modern e-beam lithography, very well defined periodic arrays of submicron antidotes [1,2,4–6] or magnetic dots [7–9] can be fabricated in a superconducting film with a low intrinsic pinning. The latter is needed to have in the film only artificial periodic pinning centers, which are well controlled. These laterally nanostructured films demonstrate sharp matching peaks in magnetization vs. field curves, corresponding to some specific vortex patterns stabilized by nanoengineered PPA. At temperatures quite close to the superconducting critical temperature,  $T_c$ , the artificial pinning sites attract the vortices very strongly and, as a result, the underlying symmetry of the pinning array dictates the symmetry of stable vortex patterns. For example, at the matching fields  $H = H_1$  and  $H = H_{1/2}$  (where  $H_1$  is the first matching field, which generates exactly one flux quantum per pinning site), square pinning array stabilizes a square vortex lattice, while in a homogeneous non-patterned reference film a conventional triangular vortex lattice minimizes the vortex-vortex repulsive interaction. Stable vortex patterns in presence of the square pinning arrays were directly visualized with a help of the Lorentz microscopy [6].

If now the vortex pinning strength in a periodic square array is smoothly reduced, we can expect that sooner or later the vortex-vortex repulsion will start to dominate

over the pinning forces and the triangular lattice can be recovered.

In the present paper we have focused on pinning phenomena in presence of a square array with a tunable pinning strength. We reveal how stable vortex configurations are evolving as a function of the pinning strength. We have found the transition lines between pinned and deformed triangular vortex lattices. At certain matching fields the vortex lattice phase diagram is more complicated due to the existence of specific periodic phase. We analyzed the phase diagrams taking into account different types of pinning potential profile. The critical current in this phase is calculated and the phase diagrams are obtained.

## II. PHASE DIAGRAM

Let us consider the two-dimensional sample with a regular square lattice of pinning sites with a period  $a$ . We assume here that the external magnetic field does not exceed the first matching field  $H_1$  and is equal to one of the sub-matching fields. It is well-known that the regular triangular vortex lattice has the lowest energy in absence of any pinning [10]. Square lattice of pinning sites can impose its own symmetry on the vortex lattice. Therefore, vortex lattice can exist in the form of at least two stable phases - pinned regular phase and triangular phase in two limiting cases (strong and weak pinning). The symmetry of the pinned lattice is not necessarily the square one. Vortex patterns corresponding to different matching fields were listed in Ref. [3] for the limit of strong pinning. Some of these patterns we also present here on Fig. 1. When the pinning strength is small it is energetically favorable to form a deformed triangular lattice. This lattice is nonregular, since triangular vortex lattice and square pinning site arrays are incommensurate. Transitions between these phases were first studied in Ref. [11] in the limit of infinitely small length scale of pinning potential well. Here we will analyze general case of an arbitrary potential well size.

The pinning energy density can be written phenomenologically as a Fourier expansion:

$$U(x, y) = \sum_{m, n} A_{mn} \cos \frac{2\pi m x}{a} \cos \frac{2\pi n y}{a}. \quad (1)$$

In the pinned regular phase all vortices are located on the pinning sites and the energy of the system  $E_1$  (per one vortex) reduces to

$$E_1 = E_{lat} + U(0,0) = E_{lat} + \sum_{m,n} A_{mn}, \quad (2)$$

where  $U(0,0)$  is the pinning potential in the center of the pinning site and  $E_{lat}$  is the energy of vortex interaction, which depends on the symmetry of the flux-line lattice (Fig. 1).

The energy of the deformed triangular lattice  $E_2$  can be found in the framework of the elasticity theory, in which a discrete vortex lattice is replaced by an elastic medium. The accuracy of such an approximation will be discussed below. The energy  $E_2$  (per one vortex) is given by

$$E_2 = E_{tr} + E_{pin} + E_{elast}, \quad (3)$$

where  $E_{tr}$  is the energy of an ideal triangular flux-line lattice,  $E_{pin}$  is the pinning energy, and  $E_{elast}$  is the energy related to the lattice distortion. To find  $E_{pin}$  and  $E_{elast}$  we should calculate first the deviations of vortices from their positions in triangular lattice. We introduce two-dimensional vector of deviation of the elastic medium  $\mathbf{u}(x, y)$ . For  $E_{pin}$  and  $E_{elast}$  we have [12]:

$$E_{elast} = \frac{S_0}{2S} \int dS \left[ (c_{11} - c_{66}) (\nabla \mathbf{u})^2 + c_{66} (\nabla_\alpha u_\beta)^2 \right], \quad (4)$$

$$E_{pin} = \frac{1}{2S} \int dS [U(x, y) - \mathbf{u}(x, y) \mathbf{f}(x, y)], \quad (5)$$

where the integration is performed over the area  $S$  of the sample,  $S_0$  is the area of the unit cell of vortex lattice, and  $\mathbf{f} = -dU/d\mathbf{r}$  is the pinning force acting on a vortex. In Eq. (5) we took into account only the first term in the energy expansion with respect to  $\mathbf{u}(x, y)$ .

The deformation  $\mathbf{u}(x, y)$  can be found by the minimization of the total energy (3). Using the Fourier representation it is easy to obtain:

$$u_{k\alpha} = -\frac{(\mathbf{k}\mathbf{f}_k)k_\alpha}{c_{11}S_0\mathbf{k}^4} - \frac{\mathbf{k}^{-2}(\mathbf{k}\mathbf{f}_k)k_\alpha - f_{k\alpha}}{c_{11}S_0\mathbf{k}^2}, \quad (6)$$

where

$$\mathbf{u}_k = \int \mathbf{u}(\mathbf{r}) e^{i\mathbf{k}\mathbf{r}} dS, \quad \mathbf{f}_k = \int \mathbf{f}(\mathbf{r}) e^{i\mathbf{k}\mathbf{r}} dS.$$

Taking into account Eq. (1) one can find the following expressions for  $\mathbf{u}(x, y)$ :

$$u_x = \frac{a}{2\pi c_{11}S_0} \sum_{m,n} A_{mn} \frac{m}{m^2 + n^2} \sin \frac{2\pi mx}{a} \cos \frac{2\pi ny}{a}, \quad (7)$$

$$u_y = \frac{a}{2\pi c_{11}S_0} \sum_{m,n} A_{mn} \frac{n}{m^2 + n^2} \cos \frac{2\pi mx}{a} \sin \frac{2\pi ny}{a}. \quad (8)$$

These expressions give the deviations of the vortices from their equilibrium positions in an ideal lattice. It should be noted that the term proportional to  $1/c_{66}$  in Eq. (6) disappears in Eqs. (7) and (8). This term corresponds to twisting of the vortex lattice. Absence of this contribution in the resulting expressions (7) and (8) implies that *regular* pinning potential *does not twist* the vortex lattice.

Note that within the elasticity theory deviations must be much smaller than the intervortex distance  $d$ , which leads to the following constraint:

$$\frac{a}{2\pi c_{11}S_0} \sum_{m,n} A_{mn} \frac{n}{m^2 + n^2} \ll d. \quad (9)$$

Now we can find  $E_{elast}$  and  $E_{pin}$  from Eqs. (4) and (5):

$$E_{elast} = \frac{1}{2c_{11}S_0} (\langle U^2 \rangle - \langle U \rangle^2), \quad (10)$$

$$E_{elast} = \langle U \rangle - \frac{1}{2c_{11}S_0} (\langle U^2 \rangle - \langle U \rangle^2). \quad (11)$$

Here we took into account the Parseval's identity

$$\sum_{m,n} A_{mn}^2 + A_{00}^2 = 2 \langle U^2 \rangle. \quad (12)$$

The elasticity energy defined by Eq. (10) is proportional to the dispersion of the pinning potential, which is a measure of deviation of function from its average value and describes its sharpness. The first term in the right-hand side of Eq. (11) corresponds to the pinning energy in the zero approximation with respect to  $\mathbf{u}(\mathbf{r})$ . In this approximation the vortex positions are independent of the pinning potential and the elastic energy equals zero. The last term describes the energy of the correlation between the vortex positions and the pinning sites. This term is equal exactly to  $-E_{elast}$  and it is cancelled in the resulting expression for the total energy:

$$E_2 = E_{tr} + \langle U \rangle. \quad (13)$$

Note that Eqs. (11)-(13) are valid for any profile of the pinning potential. For illustration of our method we show the structure of a deformed triangular lattice calculated from Eqs. (7) and (8) in Fig. 2 at  $H_1$ ,  $c_{11}S_0/U_{00} = 0.2$ ,  $\sigma = 0.1a$ . Open circles denote pinning sites, black dots - vortices.

Comparing the energy of the pinned lattice  $E_1$  with the energy of the deformed triangular lattice  $E_2$  we can obtain the criteria for the transition between them. We choose the Gaussian profile for the vortex-pinning site interaction:

$$U(x, y) = -U_0 \exp \left[ - (r/\sigma)^2 \right], \quad (14)$$

where  $U_0$  is amplitude of interaction,  $r$  is distance between vortex and the pinning site,  $\sigma$  and is the potential

length scale. The total pinning potential in the sample is equal to the sum of contributions from all pinning sites:

$$U(x, y) = -U_0 \sum_{m, n} \exp \left[ -\frac{1}{\sigma} \left( (am + x)^2 + (an + y)^2 \right) \right]. \quad (15)$$

Taking into account Eq. (15) and the following relation

$$\langle U(x, y) \rangle = -U_0 \pi \sigma^2 / a^2,$$

we equate Eqs. (2) and (13) and obtain condition of the transition between the two vortex phases:

$$U_0 = \frac{\Delta E}{\pi \frac{\sigma^2}{a^2} - \left( \sum_{m=-\infty}^{\infty} \exp \left( -\frac{a^2 m^2}{\sigma^2} \right) \right)^2}, \quad \Delta E = E_{lat} - E_{tr}. \quad (16)$$

This equation defines the boundary between the pinned lattice and the deformed triangular lattice. The phase diagram is presented in Fig. 3 in the  $U_0 - \sigma$  plane. Below the curve 1 the triangular lattice has the lower energy and upper - the pinned regular phase. The transition between these phases is discontinuous. It is clearly seen that the pinning efficiency depends not only on the amplitude of the potential but also on the size of the potential well. In fact it follows from Eq. (16) that the pinning efficiency is controlled by parameter

$$U_0 \left[ \pi \frac{\sigma^2}{a^2} - \left( \sum_{m=-\infty}^{\infty} \exp \left( -\frac{a^2 m^2}{\sigma^2} \right) \right)^2 \right].$$

The larger is the pinning site well the higher amplitude is required to stabilize the pinned phase. As we will see below, this phase diagram corresponds to the vortex lattice at all sub-matching fields not exceeding  $H_1$  ( $H_{1/8}$ ,  $H_{1/4}$ ,  $H_{3/8}$ ,  $H_{1/3}$ ,  $H_{2/3}$ ), except  $H_1$  and  $H_{1/2}$ , when phase diagrams are different.

At some specific matching fields the structure of vortex lattice can be more complicated. Below the first matching field, this happens at  $H_1$  and  $H_{1/2}$ , when pinned lattice has a square symmetry (Fig. 1(d), (e)). In this case an intermediate phase appears with decreasing pinning strength, in which vortices in odd rows are depinned and are located in the middle between pinning sites, see Fig. 4. Hence, only a half of the vortices is pinned. The existence of this phase was predicted in Ref. [11] at  $H = H_1$  for infinitely small potential well size. The symmetry of such lattice is close to the triangular one, and the enhancement of the pinning energy is compensated by the reduction of the vortex interaction energy. We analyze now the phase diagram at  $H = H_{1/2}$ ,  $H_1$  taking into consideration the existence of this state. Similar to the previous cases the energy  $E_{int}$  of the intermediate phase can be presented as

$$E_{int} = E'_{tr} + \frac{1}{2} \left( U(0, 0) + U(0, \frac{a}{2}) \right). \quad (17)$$

where  $E'_{tr}$  is the energy of the vortex interaction. Note that  $E'_{tr}$  is close to  $E_{tr}$ . The boundary between the deformed triangular lattice and the intermediate state is defined by the following equation:

$$U_0 = 2(E'_{tr} - E_{tr}) \times \left[ -2\pi \frac{\sigma^2}{a^2} + \left( \sum_{m=-\infty}^{\infty} \exp \left( -\frac{a^2 m^2}{\sigma^2} \right) \right)^2 + \sum_{m=-\infty}^{\infty} \exp \left( -\frac{(m+0.5)^2}{(\sigma/a)^2} \right) \times \sum_{m=-\infty}^{\infty} \exp \left( -\frac{m^2}{(\sigma/a)^2} \right) \right]^{-1}. \quad (18)$$

The boundary between the intermediate phase and the square pinned lattice is given by:

$$U_0 = 2(E_{sq} - E'_{tr}) \times \left[ \left( \sum_{m=-\infty}^{\infty} \exp \left( -\frac{a^2 m^2}{\sigma^2} \right) \right)^2 - \sum_{m=-\infty}^{\infty} \exp \left( -\frac{a^2 (m+0.5)^2}{\sigma^2} \right) \times \sum_{m=-\infty}^{\infty} \exp \left( -\frac{a^2 m^2}{\sigma^2} \right) \right]^{-1}, \quad (19)$$

where  $E_{sq}$  is the energy of an ideal square vortex lattice ( $E_{lat} = E_{sq}$ ).

The vortex phase diagram for  $H_1$  and  $H_{1/2}$  and is presented schematically in Fig. 5(a). This diagram is more complicated than that shown in Fig. 3. Below curve 1 the deformed triangular lattice is more favorable energetically, in the region between curves 1 and 2 - the intermediate state, and above curve 2 - the pinned square lattice. The transitions between all these phases are discontinuous. The values of  $E_{tr}$ ,  $E'_{tr}$ , and  $E_{sq}$  were calculated within the London theory at  $H = H_1$ ,  $a = \lambda$  for ( $\lambda$  is the London penetration depth). The energy is measured in units of  $H_c^2/8\pi$ , where  $H_c$  is the thermodynamic critical field.

To analyze how the phase diagram depends on the type of the pinning potential, we also calculated the diagram for the parabolic pinning well:

$$V(r) = -U_0 \left[ 1 - \left( \frac{r}{\sigma} \right)^2 \right], \text{ if } r \leq \sigma; \quad V(r) = 0, \text{ if } r > \sigma, \quad (20)$$

where  $r$  is the distance from the center of the well. In this case the following expressions define the boundaries between the triangular lattice and intermediate phase, intermediate phase and square lattice, triangular lattice and square lattice, respectively:

$$U_0 = \frac{2(E'_{tr} - E_{tr})}{1 - \pi \frac{\sigma^2}{a^2}}, \quad (21)$$

$$U_0 = 2(E_{sq} - E'_{tr}), \quad (22)$$

$$U_0 = \frac{E_{sq} - E'_{tr}}{1 - \pi \frac{\sigma^2}{2a^2}}. \quad (23)$$

The phase diagram for this potential is presented in Fig. 5(b) at  $a = 0.2\lambda$  for  $H = H_1$ . There is also the intermediate phase separating the deformed triangular and the pinned square lattices. The boundaries are represented by curves 1, 2, and 3. The main difference from the Gaussian interaction between the vortex and the pinning site is the existence of the triple point, when the size of the potential well is large.

We can conclude that for any type of the pinning potential the phase diagram of the vortex lattice at  $H_1$  and  $H_{1/2}$  in the plane pinning strength-pinning well size consists of three main regions: the deformed triangular lattice (most vortices are situated not at the pinning sites), the ordered intermediate phase (half of vortices are pinned by PPA and half are interstitials), and the pinned square lattice (all vortices are pinned by square PPA). However, details of the phase diagram depend on the exact form of the potential profile. For some types of the pinning potential the phase diagram has a triple point between these three phases, when the sizes of the potential wells are large.

### III. CRITICAL CURRENT

In this subsection we study the critical current of the sample in the intermediate phase. We consider two situations - when the external current is directed along the  $y$ - or the  $x$ -axis on Fig. 4(b). It is obvious that critical currents are different in these cases in contrast to the pinned square and the deformed triangular lattices, when they are the same in the  $x$ - and  $y$ -directions.

In fact there are two systems of the potential wells in the intermediate phase. The first one is formed by the pinning sites themselves and positions of these wells are fixed. The second one is formed due to the interaction with vortices trapped by pinning sites ("caging"). In absence of any current the second potential wells have minima at the interstitial positions, see Fig. 4(b). When the transport dc current is applied, the vortices trapped by pinning sites are displaced, and as a result, the positions of minima of the potential wells, in which interstitial vortices are situated, will also change. Therefore, displacements of both interstitial and pinned vortices depend on each other and on the parameters of the pinning potential.

Consider first the situation when the external current  $j$  flows in the  $y$ -direction and  $H = H_1$ . The Lorentz force acting on vortices is directed along the  $x$ -axis and is given by:

$$f_L = \frac{2\pi}{\kappa} j. \quad (24)$$

Here and below the dimensionless variables are used: the distance  $r$ , the magnetic flux density  $h$ , and the energy

density are measured in units of  $\lambda$ ,  $H_c\sqrt{2}$ ,  $H_c^2/8\pi$ , respectively. In this notation  $\Phi_0 = 2\pi/\kappa$ , where  $\Phi_0$  is the magnetic flux quanta. To calculate the energy of the system we use the usual London expression for the vortex field [10]:

$$b(r) = \frac{1}{\kappa} K_0(r), \quad (25)$$

where  $K_0(r)$  is the modified Bessel function,  $r$  is the distance from the vortex center. The magnetic energy of the vortex is given by [10]:

$$E_m = \frac{2\pi}{\kappa} h(0), \quad (26)$$

where  $h(0)$  is the total magnetic field in the center of vortex. This field is equal to the sum of fields of each vortex. To describe the pinning potential we use the Gaussian potential defined by Eq. (15). We denote the displacements of interstitial and pinned vortices as  $x_1$  and  $x_2$ . The energies  $F_1$  and  $F_2$  and of these vortices are given by:

$$F_1 = \frac{2\pi}{\kappa^2} \sum_{m,n} K_0 \left( \sqrt{(a + x_1 - x_2 + 2am)^2 + \left(\frac{a}{2} + an\right)^2} \right) - U_0 \sum_{m,n} \exp \left( -\frac{(x_1 + am)^2 + \left(\frac{a}{2} + an\right)^2}{\sigma^2} \right) + f_L x_1, \quad (27)$$

$$F_2 = \frac{2\pi}{\kappa^2} \sum_{m,n} K_0 \left( \sqrt{(a + x_1 - x_2 + 2am)^2 + \left(\frac{a}{2} + an\right)^2} \right) - U_0 \sum_{m,n} \exp \left( -\frac{(x_2 + am)^2 + (an)^2}{\sigma^2} \right) + f_L x_2. \quad (28)$$

We omitted all terms independent on  $x_1$  and  $x_2$  in these expressions. The vortex positions on  $x_1$  and  $x_2$  can be found from the force balance condition:

$$\frac{\partial F_1}{\partial x_1} = 0, \quad \frac{\partial F_2}{\partial x_2} = 0. \quad (29)$$

These equations can be solved numerically. As a result we can find the critical current, i.e., the maximum value of the current, at which Eqs. (29) still have solutions. The critical current dependence on the amplitude of the vortex-pinning site interaction  $U_0$  is plotted in Fig. 6 at  $\sigma = 0.1a$ ,  $a = \lambda$ . Below solid curve the vortex lattice is stable, above it becomes unstable and vortices start to move.

The situation is more complicated, if the external current flows in the  $x$ -direction, see Fig. 4(b). For this case the system of equations similar to Eqs. (27)-(29) has been solved. Our results are presented in Fig. 7. We

found that the vortex depinning transition occurs in two steps. First, the positions of interstitial vortices become unstable at some finite value of current, and they jump to the neighboring pinning sites in the  $y$ -direction. The dependence of this current on  $U_0$  is shown in Fig. 7 at  $\sigma = 0.1a$ ,  $a = 1$  (curve 1). The pinned square lattice remains stable up to the value of critical current (curve 2), which is more than two times higher than the current leading to the first instability. Thus, the phase diagram (Fig. 7) consists of three regions: phase with interstitial vortices, pinned square lattice, and moving vortices. The dependence of the critical current on  $U_0$  for this case is also presented in Fig. 6 (dot curve) for the comparison with the critical current in the  $y$ -direction (solid curve). The critical current in the first case is much higher than that in the second case. This is because for the destruction of the stable vortex configuration in the first case we need to suppress the potential wells created by pinning sites. In the second case - only effective potential wells created by the repulsion with the pinned vortices. Such a high anisotropy of the critical current is a specific feature of the intermediate phase, and it can be used for the experimental detection of this state.

Finally, we note that according to our estimates, based on the results of Refs. [13,14], the pinned phases are energetically more favorable in experiments [2–5] on the films with antidot arrays, since the pinning efficiency is very high in such systems. The triangular deformed lattice and intermediate phase can be studied in the films, where the pinning strength of the sites can be tuned, for instance, by using the periodic arrays of *blind* holes.

#### IV. CONCLUSIONS

We have studied the stable vortex configurations in a regular array of weak pinning sites at matching fields not exceeding the first matching field  $H_1$ . When the pinning efficiency is low enough it is energetically favorable to have a deformed triangular lattice, when it is sufficiently high a lattice of pinned vortices is formed. The phase diagrams of the vortex lattices are calculated in the plane of two coordinates: the amplitude of vortex-pinning site interaction and the pinning potential well size. The vortex displacements in the deformed triangular lattice with respect to the positions in an ideal one are found within the elasticity theory. When the external field is equal to the first matching field or is twice lower, the existence of the intermediate regular phase is also energetically favorable, in which half of the vortices is pinned by periodic pinning array and the vortex lattice is close to the triangular one. We analyzed the phase diagrams for this case taking into account different types of the pinning potential profile. We found that for some types of the potential the triple point can exist on the phase diagram, where deformed triangular lattice, pinned square lattice, and intermediate phase coexist. The critical current in

the intermediate phase is calculated. This current turns out to be highly anisotropic. When current flows parallel to the pinned vortices rows the depinning occurs when the Lorentz force suppresses the effective potential wells, in which caged interstitial vortices are trapped. When current flows perpendicular to the pinned vortices rows, first these effective "caging" potential wells are destroyed, and interstitial vortices jump to the neighboring vacant pinning sites. The phase diagrams for the stable vortex lattice in the plane of applied current-pinning potential amplitude are also obtained.

#### V. ACKNOWLEDGEMENTS

W. V. P. and A. L. R. acknowledge support by RFBR, Grants Nos. 00-02-18032 and 02-02-06560, by INTAS, Grants Nos. 01-2282 and YSF 01/2-58, and by the Russian State Program "Fundamental Problems in Condensed Matter Physics". The work in Leuven is supported by the IUAP, GOA, FWO-V, and ESF VORTEX programs.

- 
- [1] A.T. Fiory, A.F. Hebard, and S. Somekh, Appl. Phys. Lett. **32**, 73 (1978).
  - [2] M. Baert, V.V. Metlushko, R. Jonckheere, V.V. Moshchalkov, and Y. Bruynseraede, Phys. Rev. Lett. **74**, 3269 (1995).
  - [3] C.Reichhardt, C.J. Olson, and F. Nori, Prys. Rev. B **57**, 7937 (1998); M.J. Van Bael, L. Van Look, K. Temst, M. Lange, J. Bekaert, U. May, G. Guntherodt, V.V. Moshchalkov, and Y. Bruynseraede, Physica C **332**, 12 (2000).
  - [4] V.V. Moshchalkov, M. Baert, V.V. Metlushko, E. Rossel, M.J. Van Bael, K. Temst, Y. Bruynseraede, R. Jonckheere, Physica C **332**, 12 (2000).
  - [5] A. Castellanos, R. Wordenweber, G. Ockenfuss, A. v.d. Hart, and K. Keck, Appl. Phys. Lett. **71**, 962 (1997).
  - [6] K. Harada, O. Kamimura, H. Kasai, T. Matsuda, A. Tonomura, and V.V. Moshchalkov, Science **274**, 1167 (1997).
  - [7] J.I. Martin, M. Velez, J. Nogues, and I.K. Schuller, Phys. Rev. Lett. **79**, 1929 (1997).
  - [8] D.J. Morgan and J.B. Ketterson, Phys. Rev. Lett. **80**, 3614 (1998).
  - [9] M.J. Van Bael, K. Temst, V.V. Moshchalkov, and Y. Bruynseraede, Phys. Rev. B **59**, 14674 (1999).
  - [10] P. G. de Gennes, *Superconductivity of Metals and Alloys* (Benjamin, New York, 1966).
  - [11] V.N. Rudko, O.N. Shevtsova, and S.V. Shiyonovsky, Fiz. Nizk. Temp. **22**, 1314 (1996).
  - [12] A.I. Larkin, Zh. Eksp. Teor. Fiz. **58**, 1466 (1970).
  - [13] G.S. Mkrtchyan and V.V. Shmidt, Zh. Eksp. Teor. Fiz. **61**, 367 (1971) [Sov. Phys. JETP **34**, 195 (1972)]

- [14] H. Nordborg and V. M. Vinokur, Phys. Rev. B **62**, 12408 (2000).

## FIGURE CAPTIONS

FIG. 1. Vortex patterns corresponding to different matching fields: (a) -  $1/8H_1$ , (b) -  $1/4H_1$ , (c) -  $1/3H_1$ , (d) -  $1/2H_1$ , (e) -  $H_1$ . Open circles show positions of the pinning sites, black dots - vortices.

FIG. 2. The structure of the triangular vortex lattice, deformed by the square pinning array of Gaussian potential wells, defined by Eq. (20), at  $H = H_1$ ,  $c_{11}S_0/U_0 = 0.2$ ,  $\sigma = 0.1a$ .

FIG. 3. Phase diagram in the plane of the vortex-pinning site interaction amplitude and the pinning potential length-scale at sub-matching fields not exceeding  $H_1$ , except and  $(H_{1/8}, H_{1/4}, H_{3/8}, H_{1/3}, H_{2/3})$ . Below curve 1 the deformed triangular lattice has the lowest energy, above - pinned phase.

FIG. 4. The structure of the intermediate phase at  $H_{1/2}$  (a) and  $H_1$  (b). Black dots and open circles denote the positions of the vortices and the pinning sites. Dashed lines show the symmetry of the vortex lattice.

FIG. 5. Phase diagram in the plane of vortex-pinning site interaction amplitude  $U_0$  and the pinning potential length-scale  $\sigma$  at  $H = H_1$ . Fig. 5(a) corresponds to the Gaussian potential of the vortex-pinning site interaction, (b) - to the parabolic one. The similar phase diagrams are also valid for  $H = H_{1/2}$ .

FIG. 6. Phase diagram of the intermediate phase in the plane: applied current - amplitude of the vortex-pinning site interaction at  $H = H_1$ ,  $a = 1$ ,  $\sigma = 0.1a$ . The current flows along the  $y$ -direction in Fig. 4(b). Solid curve (critical current) shows the boundary between the stable lattice with the interstitial vortices and the moving vortices. Also shown for the comparison (dot curve) is the critical current in the  $x$ -directions in Fig. 4(b).

FIG. 7. Phase diagram of the intermediate phase in the plane: applied current - amplitude of the vortex-pinning site interaction  $H = H_1$ ,  $a = 1$ ,  $\sigma = 0.1a$ . The current flows along the  $x$ -direction. Curve 1 corresponds to the transition from the lattice with interstitial vortices to the pinned square lattice, curve 2 - to the depinning transition.

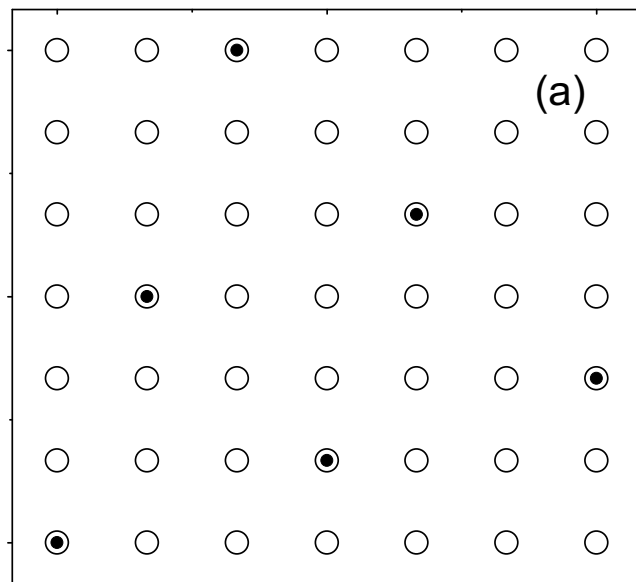


Fig. 1(a)

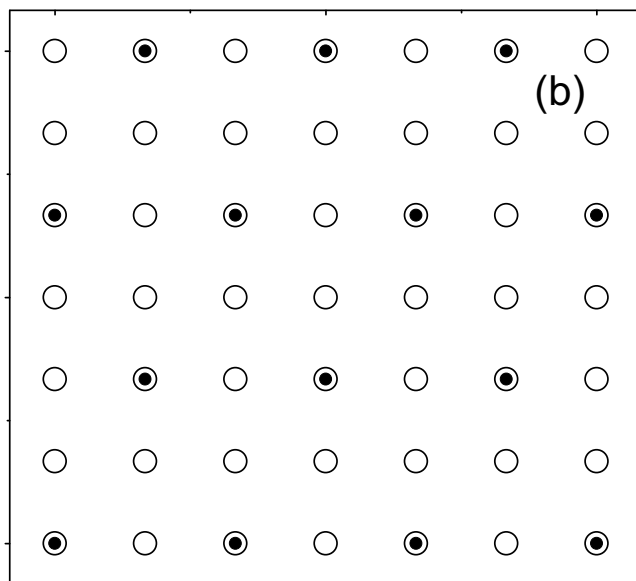


Fig. 1(b)



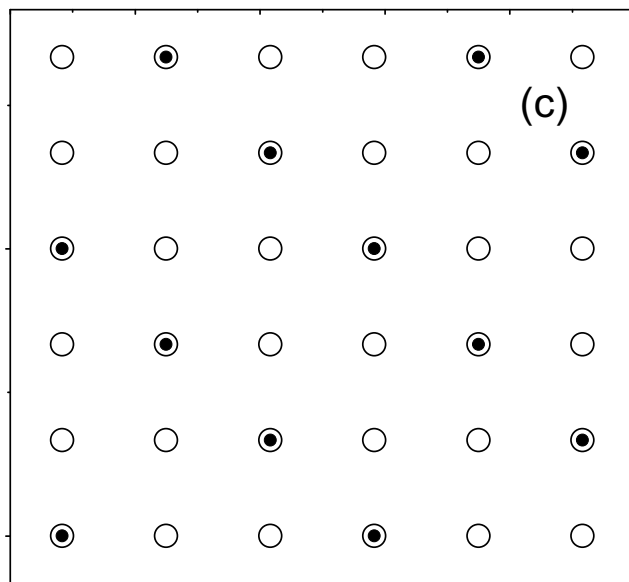


Fig. 1(c)

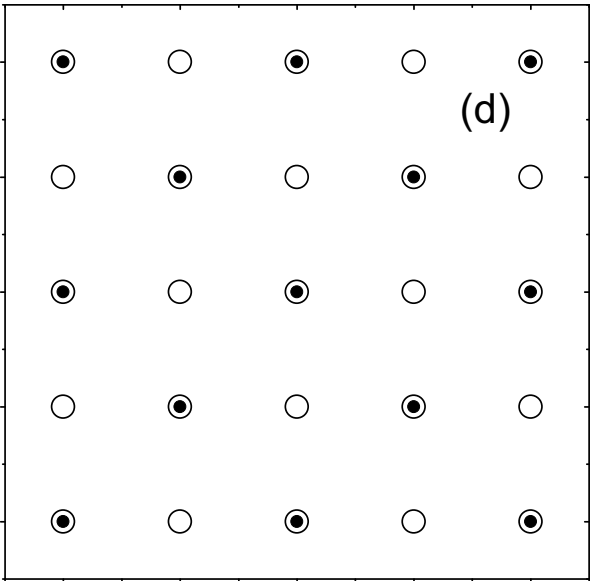


Fig. 1(d)

Fig. 1(c)

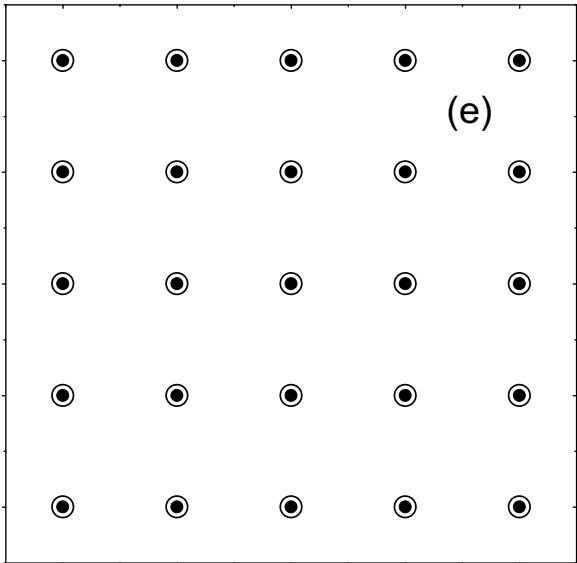


Fig. 1(e)

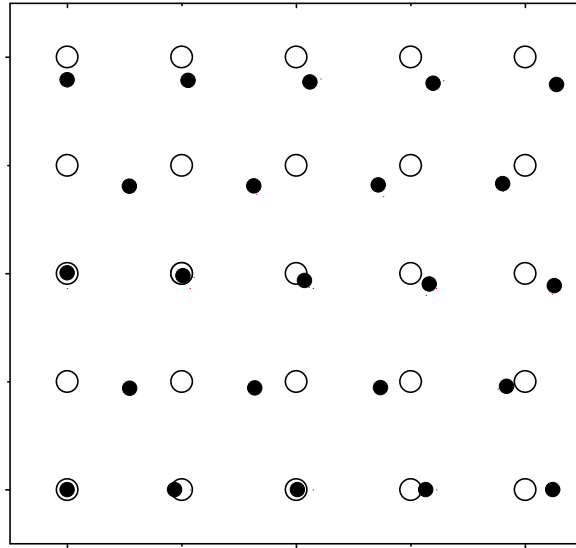


Fig. 2

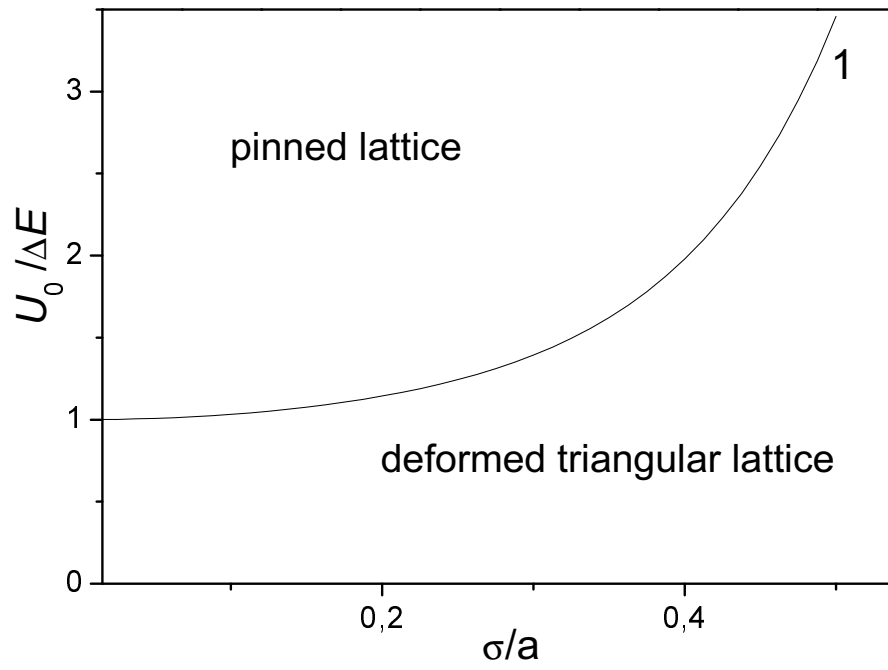


Fig. 3

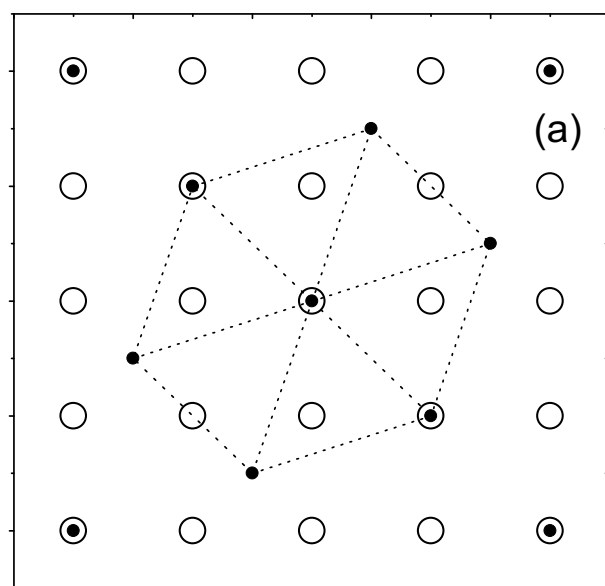


Fig. 4(a)

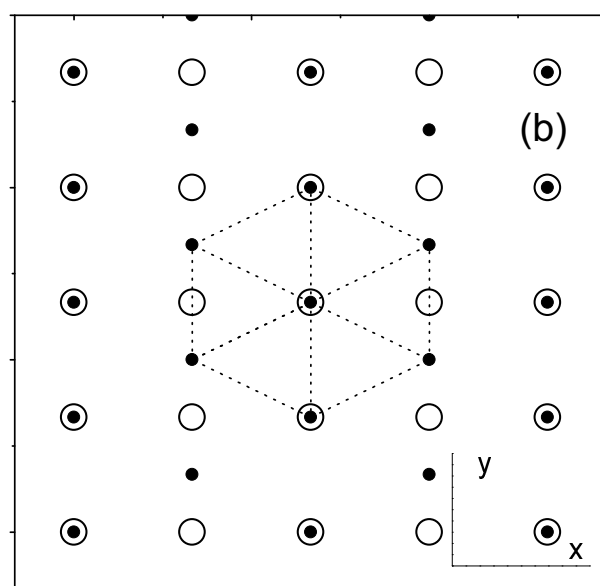


Fig. 4(b)

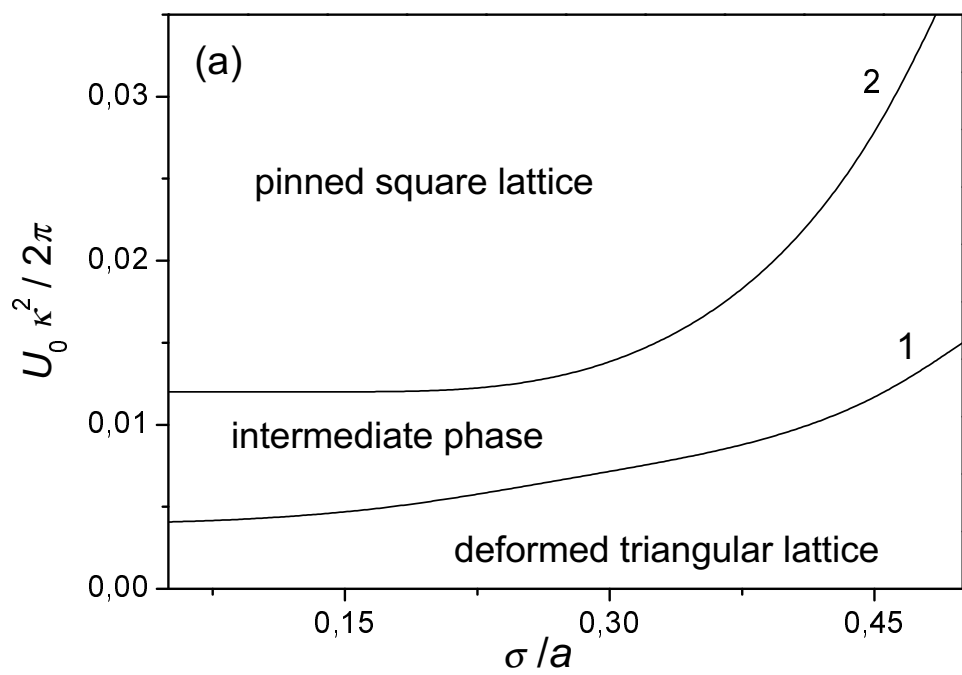


Fig. 5(a)

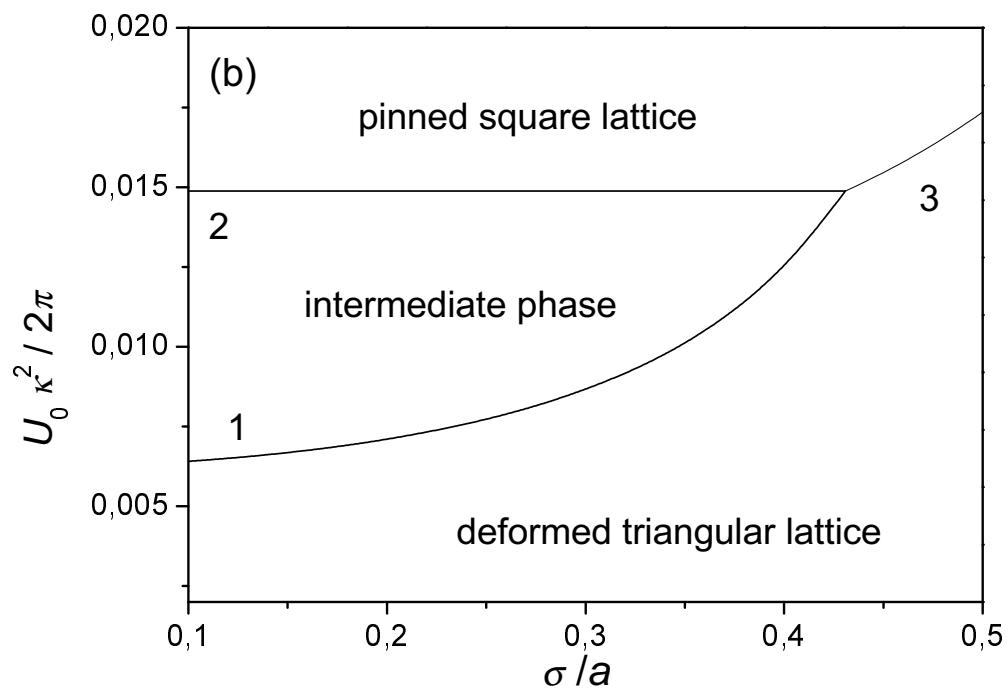


Fig. 5(b)

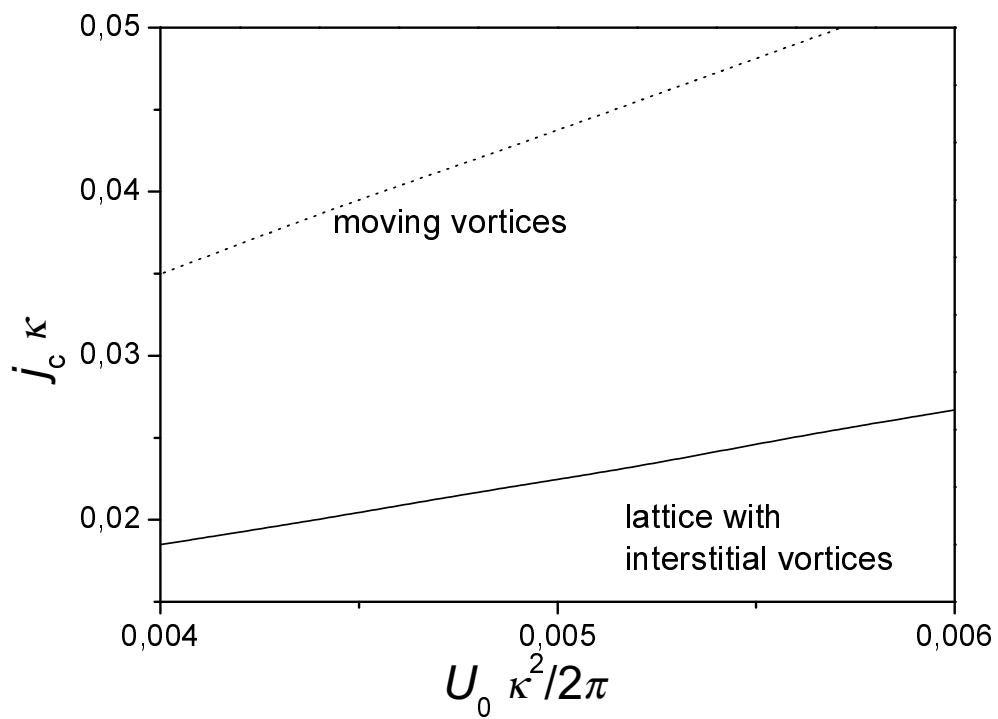


Fig. 6

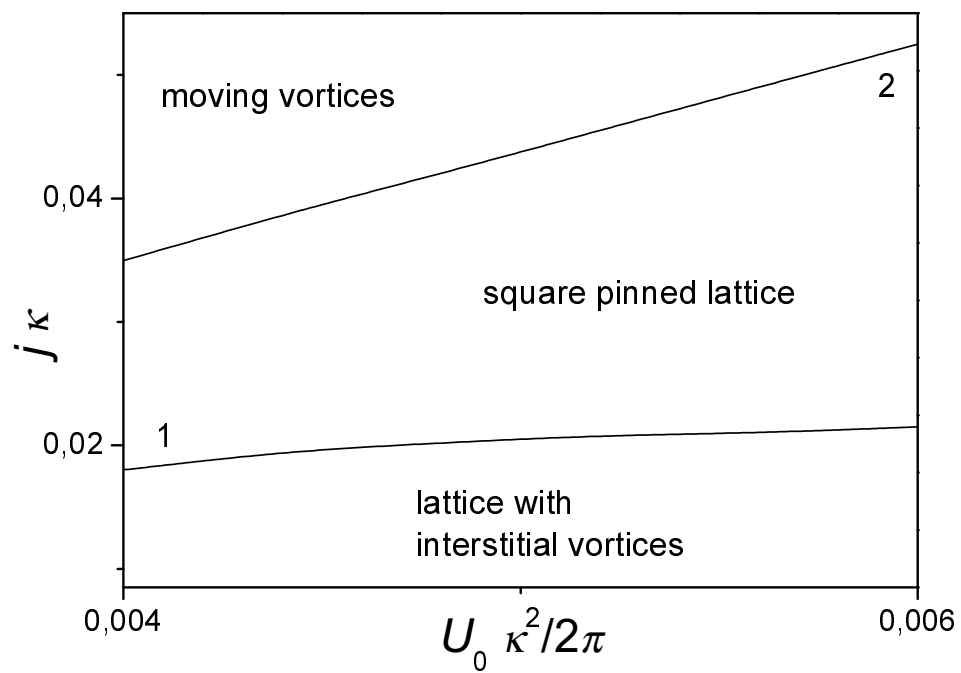


Fig. 7